European Congress on Computational Methods
in Applied Sciences and Engineering (ECCOMAS 2012)
J. Eberhardsteiner et.al. (eds.)
Vienna, Austria, September 10-14, 2012

CRACK IDENTIFICATION IN ELECTROMAGNETIC TESTING USING GENETIC ALGORITHMS BASED ON EXTENDED FINITE EDGE ELEMENTS

Jean-Charles Boisson[1], **François Lefèvre**[2], **and Stephanie Lohrengel**[2,3]

[1]CReSTIC, Université de Reims Champagne-Ardenne
Moulin de la Housse - BP 1039, 51687 REIMS cedex 2, France
e-mail:Jean-Charles.Boisson@univ-reims.fr

[2] Laboratoire de Mathématiques, Université de Reims Champagne-Ardenne
Moulin de la Housse - BP 1039, 51687 REIMS cedex 2, France
e-mail: {francois.lefevre,stephanie.lohrengel}@univ-reims.fr

[3] LAMFA CNRS 7352 , Université de Picardie-Jules Verne
33 rue Saint Leu, 80039 Amiens cedex 1, France.

Keywords: crack identification, Maxwell's equations, edge elements, extended finite elements (XFEM), genetic algorithms

Abstract. *We present an optimization procedure for the identification of cracks in structures by electromagnetic waves. The inverse problem is solved by minimizing the difference between the experimental data and the synthetic data generated from the resolution of the forward problem for a potential crack candidate. A genetic algorithm approach (GA) yields a final population of cracks close to the real crack.*

The method requires the numerical resolution of the forward problem for a great number of crack configurations. This would be highly inefficient if classical finite elements were used since every crack candidate would need a particular mesh. In our method, the forward problem is discretized by means of extended finite elements (XFEM). These elements take into account discontinuities of the computed fields on meshes which are independent of the crack geometry. Thus, a single mesh is able to deal with all crack configurations which reduces considerably the computational cost.

The XFEM-strategy based on finite edge elements in the framework of Maxwell equations is presented, and numerical examples illustrate its performance for different model problems. The GA optimization process is discussed and examples of effective crack identification are given.

1 INTRODUCTION

Electromagnetic testing is an important analysis tool in non-destructive evaluation of metallic components. Aircraft fuselage, piping systems of nuclear power plants or railroad bridges are examples of civil environments where fatigue cracks occur, and their reliable detection and identification is of utmost importance. Among the different techniques of electromagnetic testing, eddy current testing is the most standard in the inspection of conducting materials. This technique allows the detection of surface cracks which do not penetrate deep in the material. Microwave inspection has been developed in order to deal with coated surfaces or cracks filled with non-conducting materials such as rust or paint (see for example [18, 5] and references therein).

The principle of electromagnetic testing relies on the observation that a defect in the test structure results in a measurable response. From a mathematical point of view, crack detection and identification is an inverse problem which is generally ill-posed and has to be solved numerically. We distinguish essentially two types of numerical methods: on the one hand, 'semi-analytical' methods are based on the knowledge of an appropriate Green's function and lead to integral equations on the flaw (see e.g. [2, 3]). On the other, completely numerical methods aim to minimize a given cost function that measures the distance between experimental data and synthetic data resulting from the numerical resolution of a boundary value problem on the tested structure [8]. The method that we present in this communication enters within the second class. More precisely, we use a genetic algorithm (GA) approach as optimization procedure in the identification process. Genetic algorithms usually imply a large number of cost function evaluations. In the case of crack identification, the evaluation of the cost function for a crack candidate requires the numerical resolution of a boundary value problem on the cracked domain. This results in heavy computations if classical, geometry conforming, finite elements are used since every crack candidate needs a particular mesh. The computational cost can be reduced considerably if the underlying boundary value problem is discretized by means of *extended* finite elements (XFEM). These elements take into account discontinuities of the computed fields on meshes which are independent of the crack geometry. Thus, a single mesh of the unflawed domain is able to deal with all crack configurations and the costly procedure of remeshing is avoided. An XFEM-GA approach for crack identification has been developed by Rabinovich et al. [15, 16] in the context of ultrasonic testing both for the time-harmonic and transient setting.

Extended finite element methods have gathered much interest during the last ten years. The seminal paper of Moës, Dolbow, and Belytschko [13] provided the basic ideas of XFEM in the context of fracture mechanics which is the domain of predilection of extended finite elements. Several variants of XFEM have been developed since (see e.g. [10, 6, 7] among others), and the XFEM technology entered in various domains such as two-phase flows, fluid-structure interaction or dislocations. The main idea of XFEM consists in enriching the basis of a standard Lagrange Finite Element Method by a step function along the crack in order to take into account the discontinuity of the displacement field across the crack. Moreover, the singular behavior of the solution near the crack tip is taken into account by the addition of some singular functions to the discretization space.

In [11], the XFEM strategy has been extended to edge elements in order to discretize the time-harmonic Maxwell equations in a translation invariant two-dimensional setting. Edge elements are used successfully in simulations of the electromagnetic field (see [14] for the original paper by Nédélec and [12] for a general presentation in three dimensions). One essential ad-

vantage of edge elements is to ensure the continuity of the tangential component of the fields across element interfaces, whereas the normal component remains free to jump.

The present paper aims to extend the ideas of [15, 16] to electromagnetic testing procedures, and is organized as follows. In Section 2, we fix two settings of the direct problem: on the one hand, the time-harmonic Maxwell equations in a conducting medium, on the other, the second-order time-dependent Maxwell equations in a non-conducting material. In Section 3, we explain the XFEM-strategy for two-dimensional edge elements and discuss their implementation. Section 4 is devoted to numerical results for the forward problem. Finally, in section 5 we make precise the inverse problem and define different cost functions. The genetic algorithm procedure is developed in subsection 5.2 and numerical results illustrate its performance.

2 SETTING OF THE PROBLEM

Let us recall the fundamental Maxwell equations in terms of the vector functions $\mathcal{E}$ and $\mathcal{H}$, representing respectively the electric and magnetic field intensity, the electric displacement $\mathcal{D}$, and the magnetic induction $\mathcal{B}$,

$$\partial_t \mathcal{B} + \operatorname{curl} \mathcal{E} = 0, \tag{1}$$

$$\partial_t \mathcal{D} - \operatorname{curl} \mathcal{H} = -\mathcal{J}. \tag{2}$$

Equation (1) is Faraday's law and (2) is Ampère's law with the Maxwell correction. The vector field $\mathcal{J}$ represents the total current density.

These equations are completed by the divergence conditions

$$\operatorname{div} \mathcal{D} = \rho, \tag{3}$$

$$\operatorname{div} \mathcal{B} = 0, \tag{4}$$

where ρ is the charge density. (3) and (4) can be deduced from (1)–(2) under the assumption of charge conservation

$$\operatorname{div} \mathcal{J} + \partial_t \rho = 0.$$

The constitutive laws for a linear conducting material which we assume homogeneous and isotropic allow to eliminate the vector fields $\mathcal{D}$ and $\mathcal{B}$:

$$\left\{ \begin{array}{rcl} \mathcal{B} & = & \mu \mathcal{H}, \\ \mathcal{D} & = & \varepsilon \mathcal{E}, \\ \mathcal{J} & = & \sigma \mathcal{E} + \mathcal{J}_s. \end{array} \right. \tag{5}$$

Here, $\mathcal{J}_s$ is the *applied* current density. In (5), μ and ε are respectively the magnetic permeabiliy and electric permittivity of the material, whereas σ denotes its conductivity.

In this paper, we are interested in two different settings of the Maxwell equations, the time-harmonic setting in a conducting material on the one hand, and the second order transient setting in a dielectric, non-conducting material. Both settings allow to write the full Maxwell equations in terms of a reduced problem and represent simplified models of the applications we have in mind which are, respectively, eddy current and microwave testing.

2.1 Time-harmonic setting in a conducting medium

In the case where the source term varies sinusoidally in time,

$$\mathcal{J}_s = \mathfrak{Re} \left(\exp(i\omega t) \boldsymbol{J}_s(\boldsymbol{x}) \right),$$

the full Maxwell equations can be reduced to a time-harmonic setting at a single frequency $\omega > 0$. To this end, assume that all field quantities can be written as

$$\begin{aligned} \mathcal{E} &= \mathfrak{Re}\left(\exp\left(i\omega t\right)\boldsymbol{E}(\boldsymbol{x})\right), \\ \mathcal{H} &= \mathfrak{Re}\left(\exp\left(i\omega t\right)\boldsymbol{H}(\boldsymbol{x})\right). \end{aligned}$$

Eliminating the magnetic field in (1) and (2) yields

$$\operatorname{curl}\mu^{-1}\operatorname{curl}\boldsymbol{E} - \omega^2\varepsilon_\sigma\boldsymbol{E} = -i\omega\boldsymbol{J}_s \tag{6}$$

where $\varepsilon_\sigma = \varepsilon - i\sigma/\omega$.

2.2 Time-dependent setting in a non-conducting medium

If the medium is non-conducting ($\sigma = 0$), eliminating the magnetic field in (1) and (2) yields the following second-order partial differential equation,

$$\varepsilon\partial_t^2\mathcal{E} + \operatorname{curl}\mu^{-1}\operatorname{curl}\mathcal{E} = -\partial_t\mathcal{J}_s, \tag{7}$$

which has to be completed by initial conditions

$$\mathcal{E}(\boldsymbol{x},0) = \boldsymbol{E}_0(\boldsymbol{x}),\ \partial_t\mathcal{E}(\boldsymbol{x},0) = \boldsymbol{E}_1(\boldsymbol{x}). \tag{8}$$

2.3 Geometry

We consider the following two-dimensional configuration. Let Q be a convex polygon of $\mathbb{R}^2$ representing the healthy structure, and denote by Γ its boundary. Next, assume that the structure presents a one-dimensional straight crack Σ, and denote by $\Omega = Q \setminus \Sigma$ the domain outside the crack. We assume the crack to be emerging at the surface of the structure. Hence,

$$\Sigma = \{\, s\boldsymbol{x}^* + (1-s)\boldsymbol{x}_\Gamma \mid s \in [0,1] \,\}$$

where the crack tip $\boldsymbol{x}^*$ belongs to the interior of Q and $\boldsymbol{x}_\Gamma$ is a point of its boundary Γ.

On the crack, we fix a unit normal vector $\boldsymbol{n}_\Sigma$ such that $(\boldsymbol{n}_\Sigma, \tau_\Sigma)$ form a direct system, where τ_Σ is the tangential vector pointing from the crack mouth to the crack tip. We define the upper and lower part of Ω with respect to the crack line by

$$\Omega^\pm = \{\boldsymbol{x} \in \Omega \mid (\boldsymbol{x} - \boldsymbol{x}^*)\cdot\boldsymbol{n}_\Sigma \gtrless 0\}\,.$$

In a two-dimensional setting, either the magnetic or the electric field is scalar. Here, we consider the case of a scalar magnetic field, and the electric field is determined by two components. The vector and scalar two-dimensional curl-operators are defined respectively by

$$\operatorname{curl}\boldsymbol{v} = \partial_1 v_2 - \partial_2 v_1 \text{ and } \mathbf{curl}\,\varphi = \begin{pmatrix} \partial_2\varphi \\ -\partial_1\varphi \end{pmatrix}$$

for any vector field $\boldsymbol{v} = (v_1, v_2)^t$ and scalar function φ. The differential operator in (6) and (7) acting on the electric field thus reads $\mathbf{curl}\,\mu^{-1}\operatorname{curl}$.

2.4 Boundary conditions

In this paper, we address a simplified configuration in which the computational domain is limited to the controlled structure. We therefore need to make precise boundary conditions at the crack and on the boundary Γ. In general, the tangential component of the electric field is discontinuous across the crack,

$$[\mathcal{E} \times \boldsymbol{n}_\Sigma]_{|\Sigma} \neq 0 \text{ on } \Sigma, \tag{9}$$

where $[u]_{|\Sigma} = u^+_{|\Sigma} - u^-_{|\Sigma}$ denotes the jump of the quantity u across Σ. By definition, an ideal crack allows no current to pass across it which amounts to saying that

$$\mathcal{J} \cdot \boldsymbol{n}_\Sigma = 0 \text{ on } \Sigma$$

for the total current $\mathcal{J}$. From (5.3) we deduce that

$$\mathcal{E} \cdot \boldsymbol{n}_\Sigma = 0 \text{ on } \Sigma, \tag{10}$$

whenever the applied current density $\mathcal{J}_s$ satisfies $\mathcal{J}_s \cdot \boldsymbol{n}_\Sigma = 0$ on Σ. Notice that in the applications that we have in mind, the applied current density has its support outside the tested structure, and thus (10) is trivially fulfilled.

On Γ, boundary conditions are derived from transmission conditions of a more realistic configuration in which the computational domain takes into account the controlled structure as well as the surrounding domain containing the source term. Here, we chose to prescribe the tangential trace of the electric field $\mathcal{E} \times \boldsymbol{n}$ on the boundary Γ ('Dirichlet-type condition').

2.5 Variational formulations and asymptotic behavior of the fields near the crack

In this subsection, we aim to fix the functional frame of the time-harmonic and second order transient problem. Let $L^2(\Omega)$ be the space of square-integrable functions defined on Ω, and for $m \in \mathbb{N}$, denote by $H^m(\Omega)$ the usual Sobolev space of functions with square-integrable derivatives up to order m. Bold letters will be used for spaces of vector fields, e.g. $\boldsymbol{L}^2(\Omega) = (L^2(\Omega))^2$. Let us introduce the following "energy"-space,

$$\mathcal{H}(\mathrm{curl};\Omega) = \left\{ \boldsymbol{v} \in \boldsymbol{L}^2(\Omega) \,\middle|\, \mathrm{curl}\, \boldsymbol{v} \in L^2(\Omega) \right\}.$$

Vector fields in $\mathcal{H}(\mathrm{curl};\Omega)$ allow the definition of a tangential trace on parts of the boundary. We set

$$\mathcal{H}_{0,\Gamma}(\mathrm{curl};\Omega) = \left\{ \boldsymbol{v} \in \mathcal{H}(\mathrm{curl};\Omega) \mid \boldsymbol{v} \times \boldsymbol{n} = 0 \text{ on } \Gamma \right\}.$$

The variational formulation of the time-harmonic problem (6) with Dirichlet boundary condition reads

$$\begin{cases} \text{Find } \boldsymbol{u} \in \mathcal{H}(\mathrm{curl};\Omega) \text{ such that } \boldsymbol{u} \times \boldsymbol{n} = g_s \text{ on } \Gamma \text{ and} \\ \boldsymbol{a}(\boldsymbol{u},\boldsymbol{v}) - \omega^2 \boldsymbol{m}(\boldsymbol{u},\boldsymbol{v}) = -i\omega(\boldsymbol{J}_s,\boldsymbol{v})\ \forall \boldsymbol{v} \in \mathcal{H}_{0,\Gamma}(\mathrm{curl};\Omega). \end{cases} \tag{11}$$

where the sesqui-linear forms $a(\cdot,\cdot)$ and $m(\cdot,\cdot)$ are respectively defined by

$$\boldsymbol{a}(\boldsymbol{u},\boldsymbol{v}) = \int_\Omega \mu^{-1}\, \mathrm{curl}\, \boldsymbol{u}\ \mathrm{curl}\, \overline{\boldsymbol{v}}\, d\boldsymbol{x} \text{ and } \boldsymbol{m}(\boldsymbol{u},\boldsymbol{v}) = \int_\Omega \varepsilon_\sigma \boldsymbol{u} \cdot \overline{\boldsymbol{v}}\, d\boldsymbol{x}.$$

In the same way, the weak form of the transient second-order problem (7) reads

$$\begin{cases} \text{Find } \boldsymbol{u}(\cdot,t) \in \mathcal{H}(\mathrm{curl};\Omega) \text{ such that } \boldsymbol{u} \times \boldsymbol{n} = g_s \text{ on } \Gamma \times [0,T], \\ \dfrac{d^2}{dt^2}\boldsymbol{m}(\boldsymbol{u}(\cdot,t),\boldsymbol{v}) + \boldsymbol{a}(\boldsymbol{u}(\cdot,t),\boldsymbol{v}) = -(\partial_t \mathcal{J}_s(\cdot,t),\boldsymbol{v})\ \forall \boldsymbol{v} \in \mathcal{H}_{0,\Gamma}(\mathrm{curl};\Omega),\ t \in (0,T) \text{ and} \\ \boldsymbol{u}(\cdot,0) = \boldsymbol{E}_0,\ \partial_t \boldsymbol{u}(\cdot,0) = \boldsymbol{E}_1. \end{cases} \tag{12}$$

In order to describe the asymptotic behavior of the electric field near the crack, let us introduce the following singular functions near the crack tip and the crack mouth. To this end, consider local polar coordinates (r^*, θ^*) near the crack tip such that $r^* = \|\boldsymbol{x} - \boldsymbol{x}^*\|$ and $\theta^* = 0$ is the straight line that extends the crack into Ω (see figure 1). The singular function S^* at the crack tip is then defined by

$$S^*(r^*, \theta^*) = (r^*)^{1/2} \sin\left(\frac{\theta^*}{2}\right). \tag{13}$$

Notice that S^* is discontinuous across the crack since

$$[S^*]_{|\Sigma} = (r^*)^{1/2} \sin\left(\frac{\pi}{2}\right) - (r^*)^{1/2} \sin\left(-\frac{\pi}{2}\right) \neq 0.$$

At the crack mouth, the singular behavior of the electric field depends on the angle ω^+ (resp. ω^-) that the crack forms with the upper (resp. lower) part of the boundary Γ. Notice that $\omega^+ + \omega^- \leq \pi$ since Q is assumed to be convex. Hence, at most one of the two angles will be greater than $\pi/2$. To fix ideas, assume that $\omega^+ > \pi/2$. Then, the singular function associated with $\boldsymbol{x}_\Gamma$ is defined in local polar coordinates by

$$S_\Gamma(r_\Gamma, \theta_\Gamma) = \begin{cases} r_\Gamma^\lambda \sin(\lambda \theta_\Gamma) & \text{in } \Omega^+ \\ 0 & \text{in } \Omega^- \end{cases}$$

where $\lambda = \frac{\omega^+}{2\pi}$ is the singular coefficient at $\boldsymbol{x}_\Gamma$.

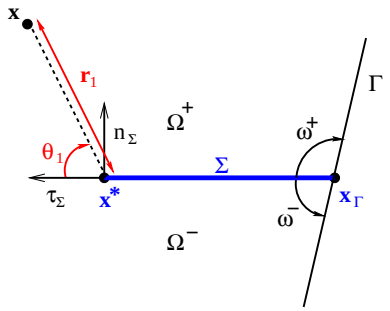

Figure 1: Local polar coordinates.

The next theorem gives the asymptotic behavior of the electric field in the case of the time-harmonic setting.

Theorem 1 *Assume that $\sigma > 0$. Under appropriate regularity conditions on the data $\boldsymbol{J}_s$ and g_s, problem (11) admits a unique solution $\boldsymbol{u} \in \mathcal{H}(\mathrm{curl}; \Omega)$ that is divergence-free in Ω and satisfies the boundary condition*

$$\boldsymbol{u} \cdot \boldsymbol{n} = 0 \text{ on } \Sigma.$$

Moreover, $\boldsymbol{u}$ splits into a regular and a singular part as follows,

$$\boldsymbol{u} = \boldsymbol{u}_r + c^* \nabla(\eta^* S^*) + c_\Gamma \nabla(\eta_\Gamma S_\Gamma) \tag{14}$$

with $\boldsymbol{u}_r \in \boldsymbol{H}^1(\Omega)$ and $c^*, c_\Gamma \in \mathbb{C}$. Here, η^* (resp. η_Γ) is a cut-off function with respect to $\boldsymbol{x}^*$ (resp. $\boldsymbol{x}_\Gamma$), and $c_\Gamma = 0$ whenever $\omega^+ < \pi/2$ and $\omega^- < \pi/2$.

The regularity conditions on g_s should allow the construction of a regular lifting such that problem (11) can be formulated equivalently as a problem with homogeneous boundary data. In particular, g_s should vanish at the crack mouth $\boldsymbol{x}_\Gamma$ in order to satisfy the compatibility conditions between traces on Σ and Γ. Theorem 1 then follows from the results in [11].

In the transient setting, similar results can be obtained.

Theorem 2 *Assume that $\sigma = 0$. Let $(\boldsymbol{E}_0, \boldsymbol{E}_1) \in \mathcal{H}(\mathrm{curl};\Omega) \times \boldsymbol{L}^2(\Omega)$ such that $\mathrm{div}\,\boldsymbol{E}_0 = \mathrm{div}\,\boldsymbol{E}_1 = 0$ in Ω. Under appropriate regularity conditions on the data $\mathcal{J}_s$ and g_s, problem (12) admits a unique solution $\boldsymbol{u} \in \mathcal{C}^0(0,T;\mathcal{H}(\mathrm{curl};\Omega)) \cap \mathcal{C}^1(0,T;\boldsymbol{L}^2(\Omega))$. $\boldsymbol{u}$ splits into a regular and a singular part as follows,*

$$\boldsymbol{u} = \boldsymbol{u}_r + c^*(t)\nabla\left(\eta^* S^*\right) + c_\Gamma(t)\nabla\left(\eta_\Gamma S_\Gamma\right) \tag{15}$$

with $\boldsymbol{u}_r \in \mathcal{C}^0(0,T;\boldsymbol{H}^1(\Omega))$ and $c^*, c_\Gamma \in \mathcal{C}^0([0,T])$.

Under similar regularity conditions on g_s as for Theorem 1, we can obtain Theorem 2 from the results in [1].

3 DISCRETIZATION BY XFEM-EDGE ELEMENTS

In order to perform discretization in space of either problem (11) or (12) by means of extended finite edge elements, let us consider a triangulation $\mathcal{T}_h = \{K_\ell\}_{\ell=1:L}$ of the *un-cracked* domain Q that satisfies the usual regularity assumptions. Let $\mathcal{E}_h$ denote the set of edges of the mesh $\mathcal{T}_h$ and let $N_h = \mathrm{card}\mathcal{E}$. Then the space of classical two-dimensional edge elements with respect to $\mathcal{T}_h$ is given by

$$\mathbf{X}_h^{\mathrm{FE}} = \mathrm{Vect}(\boldsymbol{w}_e)_{e\in\mathcal{E}} \tag{16}$$

where for any $e \in \mathcal{E}_h$, the global (vector-valued) basis function $\boldsymbol{w}_e$ is defined by

- $\boldsymbol{w}_{e|K} \in \mathcal{R}_K$ for any $K \in \mathcal{T}_h$,
- $\ell_{e'}(\boldsymbol{w}_e) = \delta_{ee'}\ \forall e' \in \mathcal{E}_h$.

Here, the local approximation space $\mathcal{R}_K$ is defined by

$$\mathcal{R}_K = \left\{ \boldsymbol{p} \in (\mathbb{P}_1(K))^2 \;\middle|\; \exists\, \boldsymbol{a} \in \mathbb{R}^2,\ b \in \mathbb{R},\ \text{s. t. } \boldsymbol{p} = \boldsymbol{a} + b \begin{pmatrix} x_2 \\ -x_1 \end{pmatrix} \right\}$$

and the linear form $\ell_e(\cdot)$ is given by

$$\ell_e(\boldsymbol{v}) = \int_e \boldsymbol{v}\cdot\boldsymbol{t}_e\, d\boldsymbol{x}$$

where $\boldsymbol{t}_e$ is the unit tangent vector of the (oriented) edge e.

Notice that classical edge elements are $\mathcal{H}(\mathrm{curl})$-conforming and thus

$$\mathbf{X}_h^{\mathrm{FE}} \subset \mathcal{H}(\mathrm{curl};Q).$$

Consequently, fields in $\mathbf{X}_h^{\mathrm{FE}}$ do not have jumps across the crack Σ. The idea of XFEM now consists in adding special fields to the classical discretization space $\mathbf{X}_h^{\mathrm{FE}}$ in order to take into account the discontinuity of the fields across the crack and its singular behavior at the crack tip and mouth. To this end, let us introduce the set of *enriched* edges by

$$\mathcal{E}^H = \left\{ e \in \mathcal{E}_h \;\middle|\; \text{the crack passes through } \Sigma \text{ such that } \mathrm{meas}(\mathrm{supp}(\boldsymbol{w}_e) \cap \Omega^{\pm}) > 0 \right\}.$$

Let $N_h^H = \mathrm{card}\mathcal{E}^H$ be the number of enriched edges and let N_S be the number of singular fields ($N_S = 1$ or $N_S = 2$).

As in [11], the enriched discretization space $\mathbf{X}_h^{\mathrm{XFEM}}$ is then defined by

$$\mathbf{X}_h^{\mathrm{XFEM}} = \mathbf{X}_h^{\mathrm{FE}} \oplus \mathrm{Vect}(H\boldsymbol{w}_e \,|\, e \in \mathcal{E}^H) \oplus \mathrm{Vect}(\nabla(\eta^* S^*), \nabla(\eta_\Gamma S_\Gamma))$$

where H is the Heaviside-like function defined with respect to the crack by

$$H(\boldsymbol{x}) = \begin{cases} +1 & \text{if } (\boldsymbol{x} - \boldsymbol{x}^*) \cdot \boldsymbol{n}_\Sigma > 0, \\ -1 & \text{otherwise.} \end{cases}$$

Notice that the enriched space $\mathbf{X}_h^{\mathrm{XFEM}}$ defines a conforming method with respect to the cracked domain Ω, i. e.

$$\mathbf{X}_h^{\mathrm{XFEM}} \subset \mathcal{H}(\mathrm{curl}; \Omega)$$

(see [11] for the proof).

3.1 Discretization of the time-harmonic problem

The discretization of the time-harmonic problem (11) results in a linear system

$$\mathbb{A}^{\mathrm{XFEM}} U^{\mathrm{XFEM}} = F^{\mathrm{XFEM}}$$

that naturally has a block structure corresponding to the classical basis functions $\boldsymbol{w}_e$, the enriched basis functions $H\boldsymbol{w}_e$ and the singular terms $\nabla(\eta^* S^*)$, $\nabla(\eta_\Gamma S_\Gamma)$:

$$\begin{bmatrix} \mathbb{A}_E & \mathbb{B}_E & \mathbb{C}_E \\ \mathbb{B}_E^T & \mathbb{A}_H & \mathbb{C}_H \\ \mathbb{C}_E^T & \mathbb{C}_H^T & \mathbb{A}_S \end{bmatrix} \begin{bmatrix} U_E \\ U_H \\ U_S \end{bmatrix} = \begin{bmatrix} F_E \\ F_H \\ F_S \end{bmatrix}. \tag{17}$$

Here, $\mathbb{A}_E \in \mathcal{M}_{N_h}(\mathbb{C})$ is the classical sparse matrix of first order edge elements,

$$(\mathbb{A}_E)ee' = \boldsymbol{a}(\boldsymbol{w}_{e'}, \boldsymbol{w}_e) - \omega^2 \boldsymbol{m}(\boldsymbol{w}_{e'}, \boldsymbol{w}_e) \, \forall e, e' \in \mathcal{E}_h,$$

whereas $\mathbb{B}_E \in \mathcal{M}_{N_h, N_h^H}(\mathbb{C})$ and $\mathbb{A}_H \in \mathcal{M}_{N_h^H}(\mathbb{C})$ involve the enriched basis functions,

$$\begin{aligned} (\mathbb{B}_E)_{ee'} &= \boldsymbol{a}(H\boldsymbol{w}_{e'}, \boldsymbol{w}_e) - \omega^2 \boldsymbol{m}(H\boldsymbol{w}_{e'}, \boldsymbol{w}_e) \, \forall e \in \mathcal{E}_h, \, \forall e' \in \mathcal{E}^H, \\ (\mathbb{A}_H)_{ee'} &= \boldsymbol{a}(H\boldsymbol{w}_{e'}, H\boldsymbol{w}_e) - \omega^2 \boldsymbol{m}(H\boldsymbol{w}_{e'}, H\boldsymbol{w}_e) \, \forall e, e' \in \mathcal{E}^H. \end{aligned}$$

Notice that $\mathbb{B}_E$ and $\mathbb{A}_H$ are also sparse matrices, and that $\mathbb{A}_H$ is extracted from $\mathbb{A}_E$ since $H^2 \equiv 1$ on Ω.

Further, $\mathbb{C}_E \in \mathcal{M}_{N_h, N_S}(\mathbb{C})$ and $\mathbb{C}_H \in \mathcal{M}_{N_h^H, N_S}(\mathbb{C})$ are coupling terms between the finite element basis functions $\boldsymbol{w}_e$ and $H\boldsymbol{w}_e$ on the one side and the singular fields $\nabla(\eta^* S^*)$ and $\nabla(\eta_\Gamma S_\Gamma)$ on the other.

Finally, $\mathbb{A}_S \in \mathcal{M}_{N_S, N_S}$ is the matrix corresponding to the singular fields. Notice that $\mathbb{A}_S$ is diagonal if the cut-off functions η^* and η_Γ have disjoint support.

In extended finite element methods, special attention has to be paid when using numerical integration in elementary computations. This issue has been addressed in detail in [11] where techniques from [6] are applied.

In the matrix of the linear system (17), the size of the block $\mathbb{A}_E$ is in general much larger than the size of the other blocks. But $\mathbb{A}_E$ is independent from the crack configuration which means that in applications with multiple crack configurations, $\mathbb{A}_E$ has to be computed only once whereas the smaller blocks $\mathbb{A}_H$, $\mathbb{B}_E$, …, will change with the crack configuration. This allows to reduce considerably the computational cost of the simulations since $N_h^H + N_S \ll N_h$: in terms of the mesh size h, we have $N_h = \mathcal{O}(h^{-2})$ whereas $N_h^H + N_S = \mathcal{O}(h^{-1})$.

3.2 Discretization of the transient problem

Discretization in space of the transient problem (12) by extended finite edge elements yields a semi-discrete problem that results in the following system of linear differential equations:

$$\begin{cases} \mathbb{M}^{\mathrm{XFEM}}\ddot{U}(t) + \mathbb{K}^{\mathrm{XFEM}}U(t) = F^{\mathrm{XFEM}} \\ U(0) = E_0,\ \dot{U}(0) = E_1, \end{cases} \tag{18}$$

where $\mathbb{M}^{\mathrm{XFEM}}$ and $\mathbb{K}^{\mathrm{XFEM}}$ are, respectively, the mass matrix and "stiffness" matrix corresponding to the bilinear forms $\boldsymbol{a}(\cdot,\cdot)$ and $\boldsymbol{m}(\cdot,\cdot)$. Both matrices $\mathbb{M}^{\mathrm{XFEM}}$ and $\mathbb{K}^{\mathrm{XFEM}}$ have the same block structure as $\mathbb{A}^{\mathrm{XFEM}}$ in (17). In (18), the notation $\dot{U}$ (resp. $\ddot{U}$) denotes the first (resp. second) derivative of the quantity $U(t)$ with respect to t, and E_0 (resp. E_1) is the coefficient vector of a suitable approximation in $\mathbf{X}_h^{\mathrm{XFEM}}$ of the initial data $\boldsymbol{E}_0$ (resp. $\boldsymbol{E}_1$).

Discretization in time is performed *via* an implicit Newmark scheme. To this end, let $N_T \in \mathbb{N}^*$ and consider an equally distributed partition of the time interval $[0,T]$ with time step $\Delta t = T/N_T$,

$$t_0 = 0 < t_1 < t_2 < \cdots < t_N = T,\ t_n = n\Delta t,\ \forall n = 0,\ldots,N_T.$$

We are looking for a sequence $(U^{(n)})_{n=0,\ldots,N_T}$ of vectors $U^{(n)} \in \mathbb{R}^{N_h+N_h^H+N_S}$ such that $U^{(n)}$ is an approximation of $U(t)$ at time $t = t_n$. The Newmark scheme depends on two real parameters $\beta \in [0, \frac{1}{2}]$ and $\gamma \in [0,1]$. In the case of the differential system (18), it may be written as follows:

$$\begin{aligned} &\left(\mathbb{M}^{\mathrm{XFEM}} + \beta(\Delta t)^2\mathbb{K}^{\mathrm{XFEM}}\right)U^{(n+1)} \\ &= (\Delta t)^2\left(\beta F^{(n+1)} + (\frac{1}{2} - 2\beta + \gamma)F^{(n)} + (\frac{1}{2} + \beta - \gamma)F^{(n-1)}\right) \\ &\quad + \left(2\mathbb{M}^{\mathrm{XFEM}} - (\frac{1}{2} - 2\beta + \gamma)(\Delta t)^2\mathbb{K}^{\mathrm{XFEM}}\right)U^{(n)} \\ &\quad - \left(\mathbb{M}^{\mathrm{XFEM}} + (\frac{1}{2} + \beta - \gamma)(\Delta t)^2\mathbb{K}^{\mathrm{XFEM}}\right)U^{(n-1)} \end{aligned} \tag{19}$$

In the numerical applications hereafter, we choose $\beta = \frac{1}{4}$ and $\gamma = \frac{1}{2}$ which results in an implicit second order scheme that is unconditionally stable. We initialize the method with $U^{(0)} = E_0$ and $U^{(1)}$ solution of the linear system

$$\begin{aligned} \left(\mathbb{M}^{\mathrm{XFEM}} + \beta(\Delta t)^2\mathbb{K}^{\mathrm{XFEM}}\right)U^{(1)} &= \left(\mathbb{M}^{\mathrm{XFEM}} - (\Delta t)^2(\frac{1}{2} - \beta)\mathbb{K}^{\mathrm{XFEM}}\right)E_0 + \Delta t\mathbb{M}^{\mathrm{XFEM}}E_1 \\ &\quad + (\Delta t)^2\left((\frac{1}{2} - \beta)F^{(0)} + \beta F^{(1)}\right), \end{aligned}$$

which yields a second order initialization error. Instead, we could have chosen a first order initialization since approximation in space is of order 1 [11].

4 NUMERICAL RESULTS

Let us illustrate the performance of XFEM-edge elements with two academic examples. The (non-cracked) computational domain Q is chosen to be the square $]-0.5,0.5[\times]-0.5,0.5[$, and the crack is given by the segment $\overline{\boldsymbol{x}_\Gamma\boldsymbol{x}^*}$ with $\boldsymbol{x}_\Gamma = (0.5, 0.15)$ and $\boldsymbol{x}^* = (0.01, 0.015)$. We consider a structured triangulation of Q of mesh size $h \approx 0.05$ (cf. figure 2). Notice that we do not take into account an eventual singularity at the crack mouth $\boldsymbol{x}_\Gamma$ since it turns out that this singularity is not physically relevant.

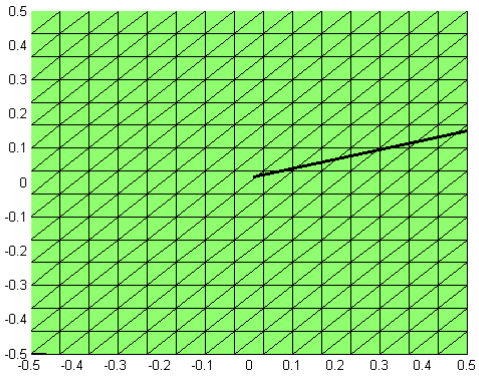

Figure 2: Triangulation of the non-cracked domain.

4.1 Time-harmonic setting

Consider problem (11) with vanishing right hand side $\boldsymbol{J}_s$ at an angular frequency $\omega = \pi/2$. The conductivity σ as well as the electromagnetic parameters ε and μ are set to 1. The problem is driven by the Dirichlet source function g_s which acts on the bottom of the boundary and is defined by

$$g_s(x,y) = \begin{cases} 1 & \text{if } y = -0.5 \\ 0 & \text{otherwise.} \end{cases}$$

In Figure 3, we represent the normal and tangential component of the real part of the electric field with respect to the crack. Notice that XFEM-edge elements reproduce rather perfectly the discontinuity of the tangential component whereas the normal component vanishes at the crack according to (9).

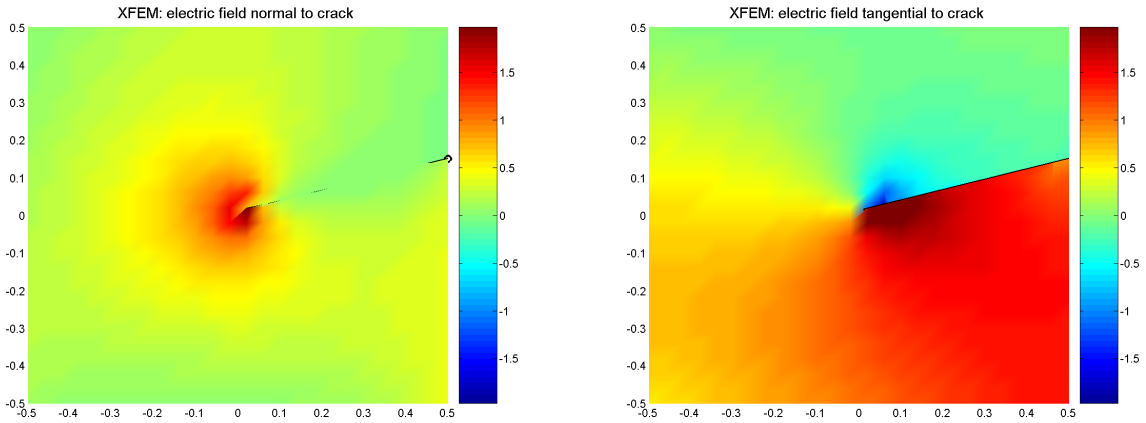

Figure 3: The electric field (real part) with source at the bottom.

4.2 Transient setting

Next, consider problem (12). Again, we set the applied current density $\mathcal{J}_s$ to zero. The transient problem is driven by the time-dependent source function

$$g_s(x,y) = \begin{cases} \chi(t)cos(\frac{\pi}{2}t) & \text{if } y = -0.5 \\ 0 & \text{otherwise.} \end{cases}$$

where $\chi(t)$ is a regular cut-off function in time such that $\chi \equiv 0$ near $t = 0$. This models a source term acting only after a short laps of time and ensures compatibility with the initial data $\boldsymbol{E}_0 = \boldsymbol{E}_1 = 0$.

The parameters of the Newmark scheme are $\beta = \frac{1}{4}$ and $\gamma = \frac{1}{2}$, and the time step is fixed as $\Delta t = 0.05$ for a total time of $T = 1$.

In Figure 4, we compare the electric field intensity $\mathcal{I}(\boldsymbol{x}, t) = |\mathcal{E}(\boldsymbol{x}, t)|^2$ in a cracked domain with the one in the non-cracked structure. We clearly observe that the perturbation due to the crack occurs after a given time $t^* \approx 0.5$ when the electromagnetic wave reaches the crack.

5 THE INVERSE PROBLEM

In this section we address the problem of crack identification from given measurements. The principal idea is the following: scattering data $\boldsymbol{m}(\Sigma)$ are obtained from the simulation of the electric field for many different crack configurations and are compared to the measured signal $\boldsymbol{m}^*$ from the crack Σ^* (which is unknown in real experiments). Then, we aim to identify Σ^* by optimizing a cost function $\mathcal{C}(\Sigma)$ related to the data $\boldsymbol{m}(\Sigma)$. The nature of the quantity $\boldsymbol{m}$ depends on the testing device and the properties of the tested body. We discuss hereafter the choice of the cost function both for the time-harmonic and transient setting. The optimization procedure itself is based on a Genetic Algorithm (GA) which will be described in Subsection 5.2.

5.1 The cost function

Impedance measurements in the time-harmonic setting

In eddy current testing, the measured quantity usually corresponds to the variation of the impedance $Z = R + i\omega L$ of the coil which induces the eddy current. The electrical resistance R of the wire is related to the heat produced by the variation of the current by Joule's law, $P = I^2 R$, where I is the current intensity of the source. On the other hand, P can be computed by

$$P = \int_\Omega \boldsymbol{J} \cdot \boldsymbol{E}\, d\boldsymbol{x},$$

where $\boldsymbol{E}$ is the solution of

$$\left\{ \begin{array}{rcll} \operatorname{curl} \mu^{-1} \operatorname{curl} \boldsymbol{E} - \omega^2 \varepsilon_\sigma \boldsymbol{E} & = & 0 & \text{in } \Omega, \\ \boldsymbol{E} \times \boldsymbol{n} & = & g_s & \text{on } \Gamma, \\ \mu^{-1} \operatorname{curl} \boldsymbol{E} \times \boldsymbol{n} & = & 0 & \text{on } \Sigma. \end{array} \right. \tag{20}$$

This finally yields, together with Ohm's law,

$$R = \frac{1}{I^2} \int_\Omega \sigma |\boldsymbol{E}|^2\, d\boldsymbol{x}. \tag{21}$$

The inductance L can be computed from the magnetic energy W by $L = \frac{2W}{I^2}$ from

$$W = \frac{1}{2} \int_\Omega \mu |\boldsymbol{H}|^2\, d\boldsymbol{x} = \frac{1}{\omega^2} \int_\Omega \mu^{-1} |\operatorname{curl} \boldsymbol{E}|^2\, d\boldsymbol{x},$$

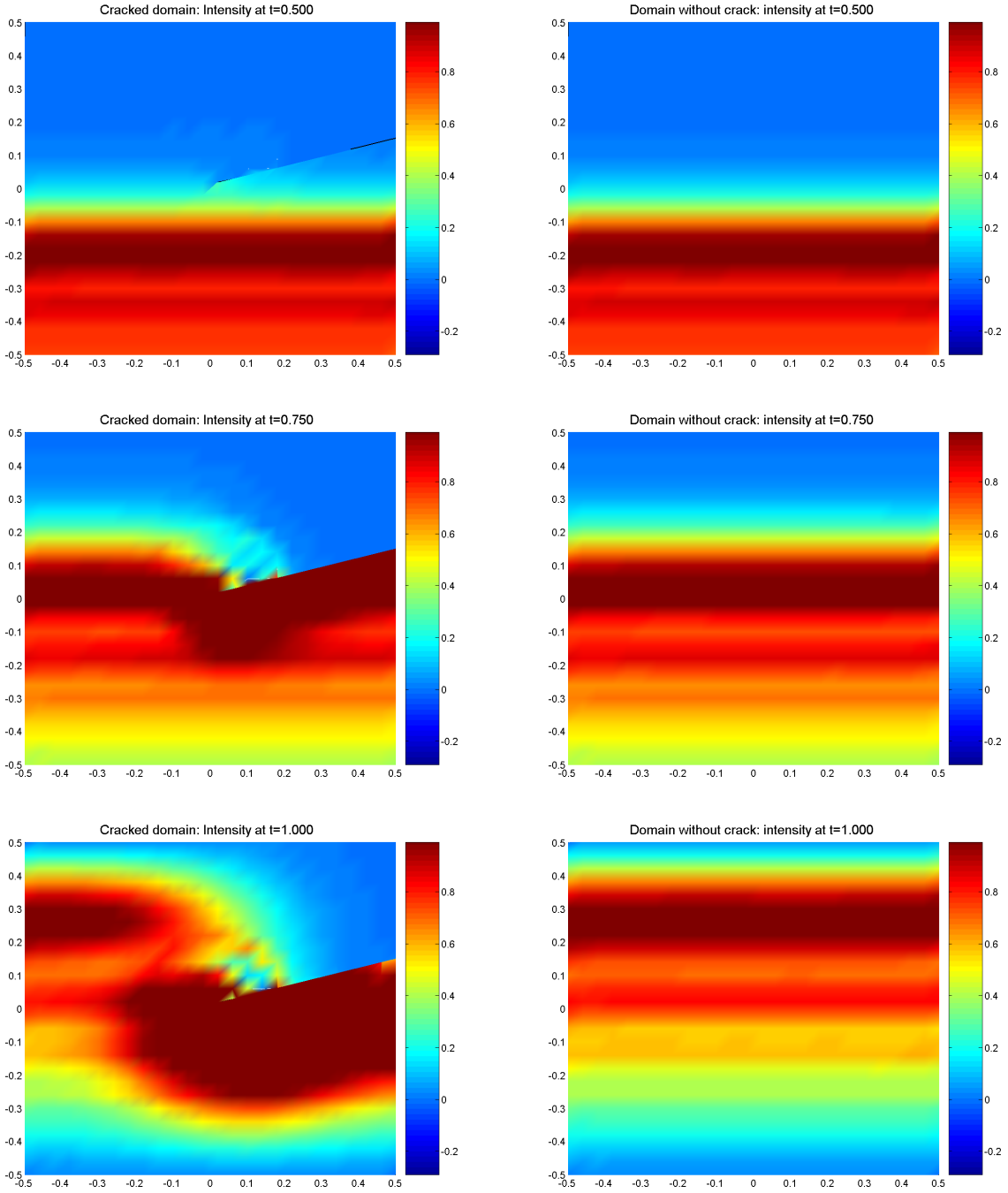

Figure 4: Evolution in time of the electric field intensity in a cracked (left column) and healthy domain (right column) with source at the bottom.

where the latter identity follows from Faraday's law (1). Notice that in eddy current devices, the computational domain usually contains both the conductor and the surrounding non-conducting medium. Consequently, the integration in (21) should be performed only over the conductor.

Now, the inverse problem of the crack identification procedure consists in minimizing the distance between the measured data Z^* corresponding to the real crack and the data Z corresponding to some crack candidate in the data base of the GA. Following [15], it is preferable

for computational reasons to maximize the following 'fitness function'

$$\mathcal{S}(\Sigma) = \frac{1}{1+\mathcal{C}(\Sigma)} \in]0,1] \tag{22}$$

where

$$\mathcal{C}(\Sigma) = \frac{|Z - Z^*|}{|Z^*|}. \tag{23}$$

Energy measurements in the transient setting

Impedance measurements are particularly adapted for eddy current testing in a time-harmonic setting. In the case of a non-conducting material, we thus have to choose a different criterion in the identification procedure. As in [15, 16], the cost function could be derived from Neumann- or Dirichlet-like data on part of the surface Γ. Actually, we chose the magnetic energy to identify the crack owing to its similarity with the impedance from a computational point of view. We thus led

$$W(t) = \frac{1}{2}\int_\Omega \mu^{-1} |\operatorname{curl} \mathcal{E}(\boldsymbol{x},t)|^2 \, d\boldsymbol{x}.$$

where $\mathcal{E}$ is the solution of

$$\left\{ \begin{array}{rcll} \varepsilon \partial_t^2 \mathcal{E} + \operatorname{curl} \mu^{-1} \operatorname{curl} \boldsymbol{E} & = & 0 & \text{in } \Omega \times (0,T), \\ \boldsymbol{E} \times \boldsymbol{n} & = & g_s & \text{on } \Gamma \times (0,T), \\ \mu^{-1} \operatorname{curl} \boldsymbol{E} \times \boldsymbol{n} & = & 0 & \text{on } \Sigma \times (0,T). \end{array} \right. \tag{24}$$

The cost function is then given by

$$\mathcal{C}(\Sigma) = \frac{\|W - W^*\|_{0,]0,T[}}{\|W^*\|_{0,]0,T[}}, \tag{25}$$

where$\|\cdot\|_{0,]0,T[}$ denotes the L^2-norm on $]0,T[$,

$$\|u\|_{0,]0,T[} = \left(\int_0^T |u(t)|^2 \, dt \right)^{1/2},$$

and the fitness function is defined by (22).

5.2 The Genetic Algorithm

Genetic Algorithms as an example of meta-heuristic methods are widely used since they are able to tackle problems with large search spaces thanks to their exploration strength. The GA designed in this work is a standard one: from an initial population and until a stopping criterion is validated, the individuals evolve by recombination and mutation to obtain better individuals [9]. In what follows, we describe the development platform of our GA and give details of its parametrization and implementation.

Development platform

For ease of the development of the GA, and in prediction of the evolution of our approach, the platform ParadisEO has been used (see [4, 17] for a detailed presentation). ParadisEO allows the design of meta-heuristic methods by simply expressing specific parts of the problem. Furthermore, these methods can be parallelized without advance work of their content.

Coding of an individual

In our approach, the GA individuals are potential cracks. The chosen representation is a set of $n \geq 2$ two-dimensional Cartesian points, $\boldsymbol{X}_c = (\boldsymbol{X}(1), \ldots, \boldsymbol{X}(n))$ with $\boldsymbol{X}(i) \in \mathbb{R}^2 \, \forall i$. Since we are mainly interested in emerging cracks, the first point of the set is constrained to lay on the boundary of the structure. The other points are situated in the interior of the domain and have to be different and distant from each other with a minimal distance depending on the mesh size. Actually we tested the approach with a set of two points corresponding to the crack mouth and crack tip.

Fitness function

As detailed in section 5.1, our GA must maximize the correlation between the candidate cracks and the experimental measures. This correlation is a real value included in the interval $[0, 1]$. The computational cost of this function depends on the size of the mesh. On the target architecture for the tests (Intel(R) Xeon(R) CPU X5650 at 2.67GHz), the computation time for one evaluation of the fitness function varied from one second to less than one minute for the different meshes and settings of the problem.

Evolving strategy

The initial population of the GA is generated randomly subject to the coding constraints. It is uniformly distributed over the computational domain. After a first evaluation, the population evolves according to a reproduction mechanism until a stopping criterion is validated. The reproduction is based on three steps: selection, crossover/mutation and replacement. The selection consists in taking two individuals, called parents, with a probability linked to their current fitness. The parents are recombined to get two new individuals, called children, thanks to a standard one-point crossover. The same cut is chosen for the two parents and the information is swapped before or after this cut to generate new individuals. With a small probability, generally 0.01, new individuals can also be mutated. In our case, a mutation consists in a little space move of a randomly chosen point of the individual. Finally, two populations co-exist: the current one and the new individuals. The generation of the next population is based on an elitist strategy. The new population contains a percentage of the best individuals of the two populations. Then the population is filled from the set of new individuals. This elitist strategy avoids to lose the best individuals and allows to keep good information contained in the other ones. Nevertheless, it can also produce premature convergence.

Stopping criteria

The standard stopping criterion for genetic algorithms is a maximal number of generations. But in the case of time and space evaluation function, a stopping criterion that manages also the convergence of the GA is a good choice. Consequently, additionally to the maximal number of generation, the evolution of the best individual fitness is used: after a minimal number of generations, the GA stops if the fitness of the best individual has not been improved during a fixed number of generations.

Parallelizing scheme

In order to work with meshes of large size in a reasonable amount of time, the evaluation of the population has been parallelized. This is the standard parallelizing scheme for genetic algorithms. The scheme is also called master/slave scheme because one resource, the master, manages the global GA while the other resources, the slaves, are waiting for evaluation tasks. In ParadisEO, the master/slave paradigm for the evaluation of a GA population is already included. It is based on the Message Passing Interface (MPI) technology and the user does not have to code it itself.

GA parameters

One of the major difficulties of genetic algorithms is the correct parametrization which plays an important role in the efficiency of the method. The two main parameters that have to be tuned are the number of generations and the computational resources that will be needed. Thanks to the ROMEO Computing Center (`https://romeo.univ-reims.fr/`), we have been able to test a large series of different configurations in order to choose the best one. After 100 executions, the chosen parameters for the number of generations are at least 10 generations followed by 15 generations without improvement of the best individual in a limit of maximal 50 generations. Consequently, the effective number of generations of each run is included in the interval $[25, 50]$. For the parallelizing scheme, the most efficient solution consists in 36 processors corresponding to 3 nodes of 12 processors on the CLOVIS cluster of the ROMEO Computing Center.

Validation protocol

The validation procedure of our approach consists in two steps. In a first time, the behavior of the different fitness functions has been tested numerically with respect to their ability to identify a given crack. Indeed, a mathematical analysis of the fitness function is often difficult and in general, the inverse problem will be shown to be mathematically ill posed. In spite of these theoretical difficulties, the feasibility of the identification process can be evaluated. To this end, heavy computations have been made which allow to check if the crack to identify is the one with the highest fitness. These computations yield landscapes that show the fitness function variations according to the shape of the cracks.

Once the fitness function is validated, at least 10 runs of the GA are used to extract valid statistics. Additionally to standard information (e.g. score of the fitness function, number of generations for convergence), we have also included the distance between the best crack found by the GA and the experimental crack which is known in the validation procedure. The distance is measured by the root-mean-square deviation (RMSD),

$$\mathrm{RMSD}(\boldsymbol{E}_c, \boldsymbol{B}_c) = \sqrt{\frac{\sum_{i=1}^{n} \|\boldsymbol{E}_c(i) - \boldsymbol{B}_c(i)\|_2^2}{n}}$$

where $\boldsymbol{E}_c = (\boldsymbol{E}_c(1), \ldots, \boldsymbol{E}_c(n))$ and $\boldsymbol{B}_c = (\boldsymbol{B}_c(1), \ldots, \boldsymbol{B}_c(n))$ are respectively representations of the experimental and the best crack and n denotes the number of points in the coding of the crack (actually $n = 2$ in our experiments).

5.3 Numerical results

In this section we present numerical results obtained with the different cost functions described in §5.1. The first configuration, called TH-I hereafter, identifies the crack from impedance measurements through the cost function (23) in a time-harmonic setting. The physical parameters ε, μ, σ and ω have been set to 1, and the source function g_s is defined by $g_s(x,-0.5) = \eta(|x-x^*|)(1+x)$ on the lower boundary of the domain. Notice the presence of a cut-off function η which vanishes near the crack mouth. This is necessary to obtain compatibility between the different boundary conditions on the outer boundary Γ and the crack Σ. We also introduced an additional term $(1+x)$ in order to avoid symmetry of the problem. The measurements Z^* have been obtained from a numerical simulation on the same mesh as the one that is used in the identification process (an 'inverse crime' according to [15]). Notice that only two measured values, the real and the imaginary part of the impedance, are sufficient to identify the crack.

In the TS-E and TS-ER configuration, we used the energy cost function (25) to identify the crack in a transient setting. Here, σ is set to 0, the final time is $T = 1$, and the time-depending source function g_s is defined by $g_s(x,-0.5,t) = \chi(t)\cos(\frac{1}{2}\pi t)\eta(|x-x^*|)(1+x)$ for $t \in (0,1)$. Whereas the measurements W^* in the TS-E configuration have been obtained on the mesh of the identification process, they have been computed on a finer mesh in the TS-ER setting.

In table 1 hereafter, we give the statistics for the different settings. Due to the small number of measurements, the identification process for the TH-I configuration yields a more important error (mean RMSD of 0.6, compared to ≈ 0.1 for the other examples). We also can notice that the number of generations before convergence is significantly higher than in the TS-E and TS-ER setting (mean number equal to 36, compared to ≈ 20). These results could probably be improved by using different frequencies which would allow to collect a larger number of measurements.

One can observe that the fitness function in the TS-ER setting is less performing than in the TS-E case. Nevertheless, comparing the RMSD and the generation number of the TS-E and TS-ER configuration shows that the performance of our approach is of the same order in both configurations.

The evolution of the populations throughout a GA run is illustrated in Figure 5. Starting from a uniformly distributed population (left column in Fig. 5), the individuals concentrate finally at the exact crack position with more or less error (right column in Fig. 5). It turns out that the TS-E setting does perform the best. This is not surprising since the number of measurements (equal to the number of times steps) is much bigger than in the TH-I setting and measured data are obtained by simulation on the mesh of the identification process resulting in a higher sensibility of the fitness function than in the 'real condition experiment' TS-ER.

6 CONCLUDING REMARKS

The present paper is a contribution to the development of computational tools for non-destructive electromagnetic testing. The identification of cracks in a two-dimensional test specimen is performed *via* a genetic algorithm based on extended finite edge elements. The use of these elements allows to maintain the computational cost at a reasonable level since the evaluation of all individuals of the GA can be done with the same (structured) mesh. We tested our approach in the time-harmonic and in the transient setting, adapting the fitness function to each configuration. The numerical results are promising since the method was able to reconstruct approximatively the exact crack shape in a reliable manner.

The present results could be probably improved in several ways: it turns out that the choice

Table 1: Statistics of the different configurations: TH-I for time-harmonic with impedance, TS-E for transient setting with energy and TS-ER transient setting with energy in real condition.

		TH-I	TS-E	TS-ER
Individual fitness	Maximum	0.99	0.99	0.92
	Minimum	0.92	0.95	0.92
	Mean	**0.95**	**0.98**	0.92
	Standard deviation	0.02	0.01	0.00
Individual RMSD	Maximum	0.96	0.75	0.23
	Minimum	0.13	0.01	0.10
	Mean	0.60	**0.14**	**0.15**
	Standard deviation	0.30	0.22	0.04
Number of generations	Maximum	50	35	31
	Minimum	12	10	13
	Mean	36	**21**	**20**
	Standard deviation	12	8	6

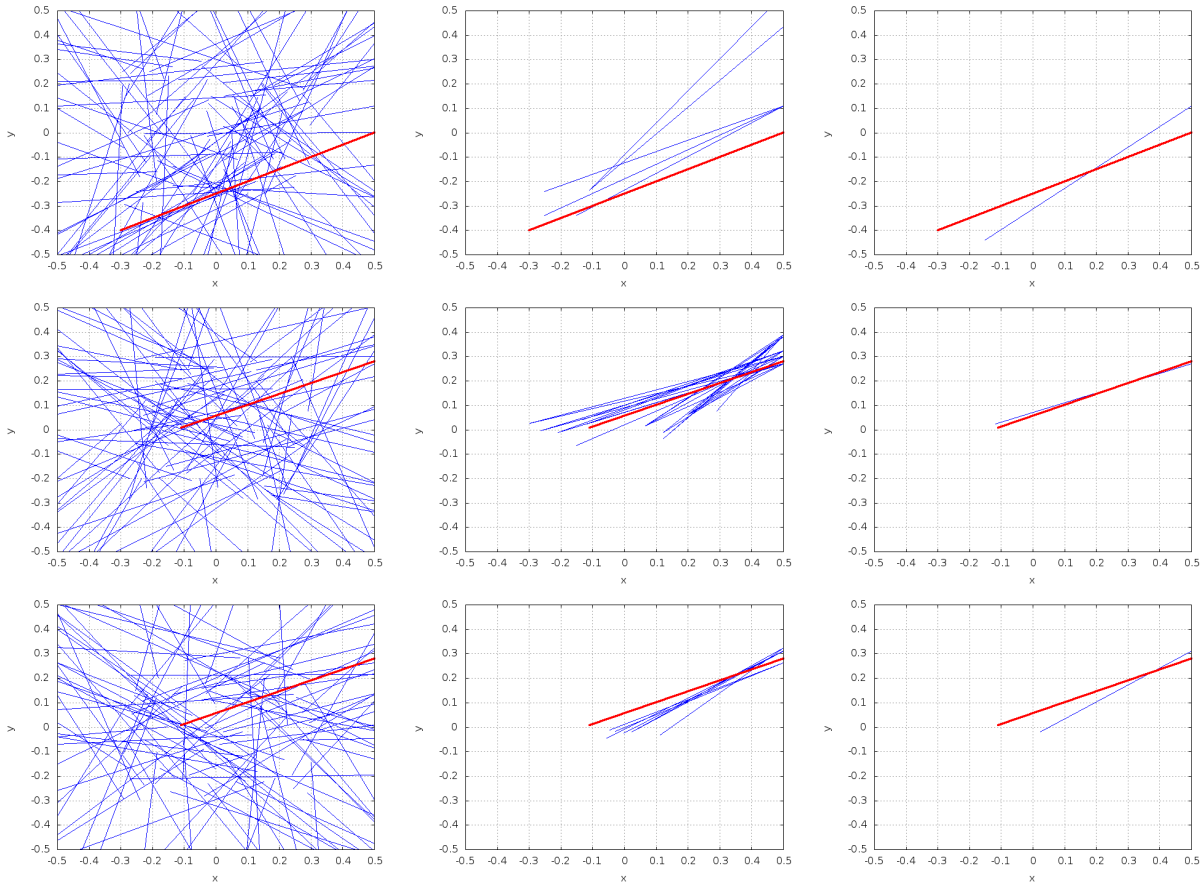

Figure 5: Evolution of the populations for the different settings: initial, intermediate and final population for time-harmonic setting with impedance (first row), transient setting with energy (second row), and transient setting with energy in real condition (last row). Exact crack in boldface red.

of the fitness function is of great importance in the setting of the inverse problem. In [16], the concept of the 'arrival-time' of the acoustic wave allowed to improve the sensitivity of the fitness function, and it would be interesting to develop a similar approach for electromagnetic waves. In eddy current testing, however, the most standard technique keeps identification from impedance measurements since no wave propagation does occur in the conductor.

From a computational point of view, a comparison of different meta-heuristic methods could be set up without conceptional difficulties thanks to the platform ParadisEO. This could point out efficient alternatives to the use of genetic algorithms in the identification process.

Currently, we are studying the extension of our approach to eddy current testing in realistic 2D and 3D configurations.

REFERENCES

[1] F. Assous, P. Ciarlet Jr.: Quelques résultats sur la régularité en temps des équations de Maxwell instationnaires, *C. R. Acad. Sci. Paris*, 327, Série I (1998), 719–724.

[2] J.R. Bowler: Thin-skin eddy-current inversion for the determination of crack shapes, *Inverse Problems*, 18 (2002), 1890–1905.

[3] J.R. Bowler, Y. Yoshida, N. Harfield: Vector-Potential Boundary-Integral Evaluation of Eddy-Current Interaction with a Crack, *IEEE Trans. Magn.*, 33 (1997), 4287–4297.

[4] S. Cahon and N. Melab and E-G. Talbi: ParadisEO: A Framework for the Reusable Design of Parallel and Distributed Metaheuristics, *Journal of Heuristics*, 3 (2004), 357-380.

[5] S. Caorsi, A. Massa, M. Pastorino, M. Donelli: Improved Microwave Imaging Procedure for Nondestructive Evaluations of Two-Dimensional Structures, *IEE Trans. Ant. Prop.*, 52 (2004), 1386–1397.

[6] E. Chahine, P. Laborde, Y. Renard: Crack tip enrichment in the XFEM method using a cut-off function, *Int. J. Numer. Meth. Engng.*, 75 (2008), 629–646.

[7] E. Chahine, S. Nicaise, and Y. Renard: Optimal convergence analysis for the extended finite element method, *Int. J. Numer. Meth. Engng.*, 86 (2011), 528–548.

[8] Y. Choua, L. Santandrea, Y. Le Bihan, C. Marchand: Specific Developments on a Finite Element Tool for Thin Crack Modeling in EC Testing, *Proceedings of the 9th European Conference on NDT*, Berlin, 2006.

[9] J. Holland: Adaptation in Natural and Artificial Systems, University of Michigan Press, 1975.

[10] P. Laborde, Y. Renard, J. Pommier, and M. Salaün: High Order Extended Finite Element Method For Cracked Domains, *Int. J. Numer. Meth. Engng.*, 64 (2005), 354–381.

[11] F. Lefèvre, S. Lohrengel, S. Nicaise: An eXtended Finite Element Method for 2D edge elements, *Int. J. Numer. Anal. Model.*, 8 (2011), 641–666.

[12] P. Monk: Finite Element Methods for Maxwell's Equations, Oxford University Press, 2003.

[13] N. Moës, J. Dolbow, J., and T. Belytschko: A finite element method for crack growth without remeshing, *Int. J. Numer. Meth. Engng.*, 46 (1999), 131–150.

[14] J. C. Nédélec: Mixed finite elements in $\mathbb{R}^3$, *Numer. Math.*, 35 (1980), 315–341.

[15] D. Rabinovich, D. Givoli, S. Vigdergauz: XFEM-based crack detection scheme using a genetic algorithm, *Int. J. Numer. Meth. Engng.*, 71 (2007), 1051–1080.

[16] D. Rabinovich, D. Givoli, S. Vigdergauz: Crack identification by 'arrival time' using XFEM and a genetic algorithm, *Int. J. Numer. Meth. Engng.*, 77 (2009), 337–359.

[17] E.-G. Talbi: Metaheuristics: From Design to Implementation, Wiley, 2009.

[18] R. Zoughi, S. Kharkovsky: Microwave and millimetre wave sensors for crack detection, *Fatigue Fract. Engng. Mater. Struct.*, 31 (2008), 695–713.